DOI: 10.31276/VJSTE.65(1).09-13

Fabrication, structural characteristics, and influence of Bi^{3+} doping concentration on UV-vis spectra of Bi^{3+}:SnO_2 nanocomposite materials

Thi Thu Hien Le[1*], Van Tuan Chu[1], Van Tuan Pham[2]

[1]Hung Yen University of Technology and Education, Dan Tien Commune, Khoai Chau District, Hung Yen Province, Vietnam
[2]International Training Institute for Materials Science (ITIMS), Hanoi University of Science and Technology, [1]Dai Co Viet Street, Hai Ba Trung District, Hanoi, Vietnam

Received 25 January 2022; accepted 5 April 2022

Abstract:

The authors report the characteristics and optical properties of Bi^{3+}-doped SnO_2 quantum dots prepared by sol-gel and hydrothermal methods. The structure and morphology of the materials as a function of doping concentration were studied and analysed by X-ray diffraction (XRD) and scanning electron microscope (SEM). The structure of the material was assigned to the tetragonal crystal structures of the SnO_2 rutile phase, reported in JCPDS Card No. 41-1445. With the increase of Bi^{3+} doping, the crystallinity of Bi-doped SnO_2 worsened. The average sizes of the SnO_2 nanocrystals were within 3-8 nm. The effect of Bi^{3+} ion concentration on the absorbance properties of the materials was investigated by UV-Vis absorption spectra. The absorbance decreased with increasing the concentration of Bi^{3+} dopant in the SnO_2 lattice. The bandgap width decreased with Bi^{3+} dopant concentration. All Bi^{3+}-doped SnO_2 samples presented an enlargement of the light absorption range due to a bandgap width decrease.

Keywords: **Bi^{3+} doped SnO_2, photocatalysis, SnO_2 nanoparticle.**

Classification numbers: **2.1, 2.3**

1. Introduction

The rapid expansion of industrialization and population worldwide has led to increasing environmental crises and energy shortages [1, 2]. Environmental chemicals or persistent organic pollutants, which are produced every day, are not only dangerous to ecological equilibrium but can also lead to various health issues affecting humans [3, 4]. Thus, removing pollutants from wastewater has attracted intense research worldwide [5]. There are various treatment methods that have been developed such as chemical oxidation, coagulation, filtration, precipitation, ion exchange, biosorption, adsorption, reverse osmosis, and photocatalytic decay...[6-13]. Photocatalysis is a notable method of removing pollutants from wastewater with its low cost, high efficiency, and environmentally friendly properties. Photocatalysis uses energy from light with the help of semiconductor photocatalysts to carry out redox reactions on its surface thereby speeding up the rate of chemical reactions. Under sunlight irradiation, electrons in semiconductors absorb photons, produce photo-electron pairs, and move to the surface of the semiconductor where redox reactions take place through which organic pollutants are accelerated to decay into carbon dioxide and water [13, 14]. However, to achieve high efficiency and energy savings, semiconductor photocatalysts need to be low cost, non-toxic, stable in water, and have a wide absorption band that includes the visible light region [15].

Tin oxide (SnO_2) is an n-type semiconductor with a wide bandgap of approximately 3.6 eV and a high exciton binding energy of approximately 130 meV [16]. With excellent electrical, optical, and chemical properties, tin oxide has been applied to solar cells [17], transparent electrodes [18], catalytic materials [19], and solid-state chemical sensors [20]. Notably, tin oxide has been used as a catalyst and support for the catalyst in several organic reactions from its high acidity [21-23]. However, due to its wide bandgap, the absorption band of SnO_2 is in the ultraviolet region. Besides, the high recombination rate for electron-hole pairs makes the photocatalytic performance of SnO_2 not as high as expected [13]. To solve this problem, one proposed solution is doping SnO_2 with metal cations to narrow the bandgap and widen the absorption band. Cation metals have a low valance that accepts electrons and not only do they resist the recombination of photo-electron pairs, but they also create oxygen vacancies in the host lattice [24]. Therefore, the photocatalytic performance of doped SnO_2 material could be improved.

[*]Corresponding author: Email: hienle585@gmail.com

According to prior research, many metals have already been used to dope SnO_2 such as Ce [6], Bi [25], Co [26], Ag [21, 27], Ni [28, 29], Cr [15], Zn [30], and Ti [5]. Among these, bismuth-based semiconductors have the potential to increase the mobility of photoelectron carriers and reduce the bandgap [31, 32]. Bismuth has electronic structures in the 6s valence band, which is well dispersed in Bi^{3+}-doped compounds and has the potential to increase the mobility of photoelectron carriers and reduce the bandgap enough to cause the absorption to extend to longer wavelengths [14, 33].

In this work, sol-gel and hydrothermal methods were utilised to fabricate Bi^{3+}-doped SnO_2 nanocomposite materials. The structural and morphological characteristics of the materials were investigated using XRD and SEM. The effects of Bi^{3+} ion concentration on optical absorption characteristics of samples were studied using ultraviolet-visible absorption spectroscopy (UV-Vis).

2. Experimental design

The Bi^{3+}:SnO_2 nanocomposite materials were prepared by sol-gel and hydrothermal methods, which are described in Fig. 1.

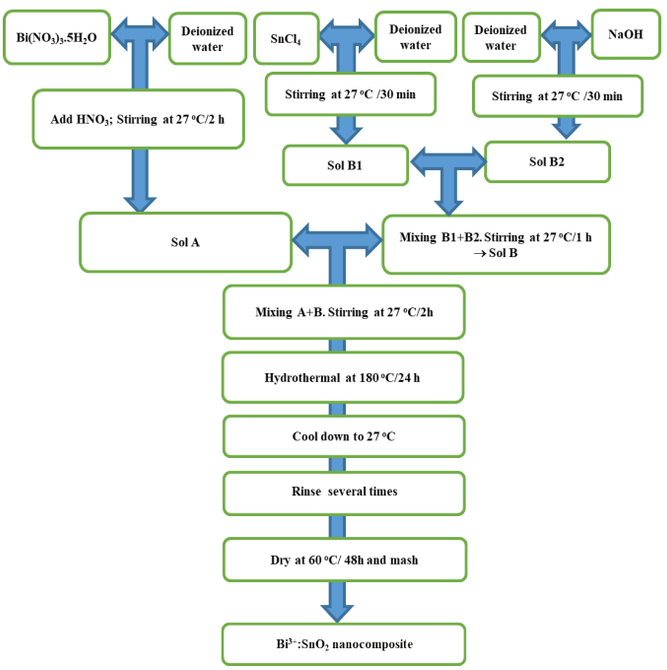

Fig. 1. Diagram of Bi^{3+}-doped SnO_2 nanocomposite synthesis.

Firstly, bismuth nitrate pentahydrate ($Bi(NO_3)_3.5H_2O$) was mixed with deionised water and stirred at room temperature for 10 min. Then, a sufficient amount of nitric acid HNO_3 was added to the mixture to form a transparent solution (sol A). Secondly, tin tetrachloride ($SnCl_4.5H_2O$, ≥98%) was mixed with deionised water and stirred at room temperature for 30 min to prepare sol B1. Sodium hydroxide (NaOH, ≥98%) was mixed with deionised water and stirred under the same condition as sol B1 for 30 min to prepare sol B2. Subsequently, the B1 and B2 sols were slowly mixed and stirred at room temperature for 1 h to prepare sol B. Thirdly, the A and B sols were slowly mixed and stirred for 2 h to form a homogeneous mixture. The last sol was infused into Teflon and the hydrothermal process began at 180°C for 24 h. After the hydrothermal process, the sample was cooled down to room temperature. The sample was then filtered and rinsed several times with deionised water and ethanol (C_2H_5OH) by centrifuge. Finally, the sample was dried and mashed to obtain Bi^{3+}:SnO_2 powder. The samples with different Bi mass ratios (4, 8 wt%) were synthesised and labelled as 4Bi-96SnO_2 and 8Bi-92SnO_2, respectively. A similar procedure was used to synthesise pure SnO_2 nanoparticles without the addition of $Bi(NO_3)_3$.5H2O, which was labelled 0Bi-100SnO_2.

All chemicals were purchased from Merck and Sigma Aldrich. XRD measurements were performed at room temperature with a Siemens D5000 (Germany) apparatus with CuK_α radiation of wavelength λ=0.154 nm. SEM images were acquired by employing an S4800-Hitachi (Japan) SEM. The absorption properties were studied using a V-650 UV-vis spectrophotometer (Jasco, USA).

3. Results and discussion

The crystalline structure and phase content of the 0, 4, and 8% Bi^{3+}:SnO_2 samples were analysed by XRD and are shown in Fig. 2. In the figure, it is seen that the crystallisation of the SnO_2 in the materials is good. Diffraction peaks were assigned to the tetragonal crystal structures of the SnO_2 rutile phase, which are in good agreement with JCPDS Card No. 41-1445, and can be observed in the XRD patterns of all the samples. Diffraction peaks at 2θ=26.392, 33.717, 37.856, 51.631, 65.904, and 78.376 correspond to (110), (101), (200), (211), (112), and (321) lattice planes, respectively. The positions of the peaks were unchanged at different Bi mass ratio samples. Peaks corresponding to Bi or Bi_2O_3 phase were not observable. This revealed that Bi^{3+} dopants could be distributed in the SnO_2 nanoparticles to form a Bi-Sn-O solid solution [6]. The crystallinity of the samples was affected by doping Bi into the SnO_2 host lattice. The intensities of diffraction peaks decreased with the increase of Bi doping amount, demonstrating that doping with Bi^{3+} form defects in the system that

prevent crystal growth [34]. The average crystal size of SnO_2 nanocrystals were estimated by using the Debye-Scherrer equation with a shape factor of 0.9 as shown in Table 1. The results showed that the average size of crystals was approximate 3-8 nm. Additionally, the half-peak maximum width tended to increase slightly. Therefore, the average crystallite size of the obtained samples decreased as the Bi^{3+} doping concentration increased. Due to their small size, the surface-to-volume ratio was increased and created more oxygen vacancies increasing the catalytic efficiency of the material [6, 27].

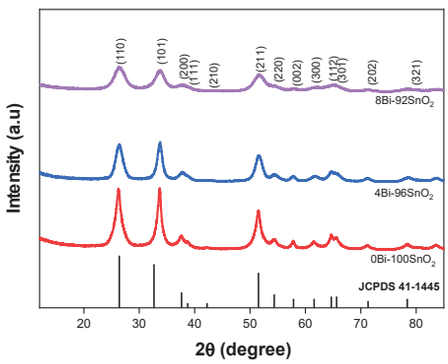

Fig. 2. XRD patterns of Bi^{3+}-doped SnO_2 nanocomposites with different Bi^{3+} mass ratios (0, 4, 8 wt%). Diffraction peak positions of SnO_2 are taken from JCPDS Card No.41-1445.

Table 1. XRD data and crystallite size of SnO_2 particles.

Bi^{3+} ratio (%W)	Peaks	2θ	FWHM	D (nm)
0	Peak 1(100)	26.243	1.599	5.33
	Peak 2 (101)	33.634	1.140	7.61
4	Peak 1(100)	26.392	1.629	5.23
	Peak 2 (101)	33.717	1.185	7.32
8	Peak 1(100)	26.457	2.51	3.40
	Peak 2 (101)	33.709	2.332	3.72

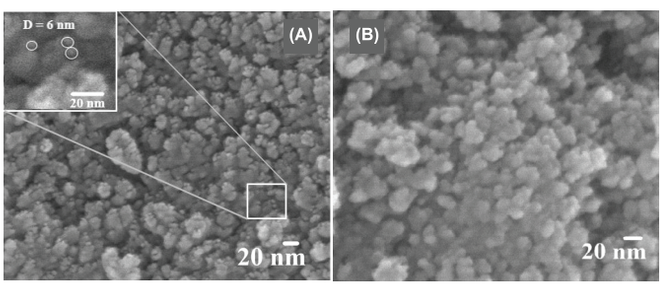

Fig. 3. SEM images of (A) pure SnO_2 and (B) 4Bi-96SnO_2. The inset shows a small area in the large-scale image.

Figure 3 presents the SEM images of pure SnO_2 and 4Bi-96SnO_2. Figs. 3A, 3B show the average size of pure SnO_2 and 4Bi-96SnO_2 is approximately 6 nm. These observations were consistent with the XRD results.

The optical absorption properties UV-Vis of the as-obtained 0, 4, and 8% Bi^{3+}-doped SnO_2 nanocomposites in the range from 200 nm to 800 nm are shown in Fig. 4. The UV-Vis spectrum showed that there was a strong absorption peak at 300 nm, which was the absorption peak of SnO_2. In addition, an absorption band between 280 and 350 nm that is characteristic of SnO_2-containing storage materials was also observed. The absorbance decreased with increasing the concentration of Bi^3dopant$^+$ in the SnO_2 lattice. This can be explained by the fact that light absorption of the Sn^{4+} ions was prevented by the Bi^{3+} impurity centres [13, 24]. The presence of Bi^{3+} created defects in the crystal lattice of the storage material thereby redistributing the atomic orbitals. There were a lot of free electrons, which appear with high mobility reducing the number of electrons at the ground level, therefore the absorbance of materials decreased. The bandgap energy (E_g) of the as-produced samples was estimated using Tauc's model:

$$(\alpha h\nu)^n = A(h\nu - Eg)$$

where α, hν, Eg, n, and A are the absorption coefficient, incident photon energy, energy gap, n (which depends on the nature of the energy transition, e,g., n=1/2 for the direct bandgap and n=2 for the indirect bandgap) and the proportionality constant, respectively [34, 35].

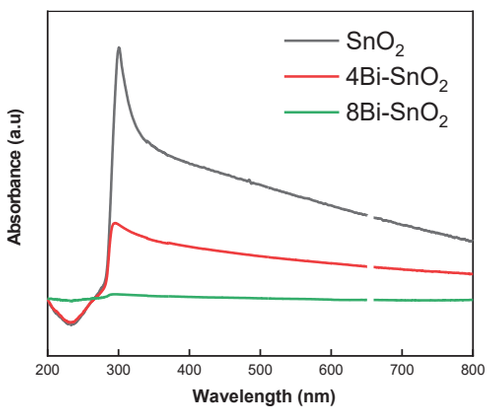

Fig. 4. UV-Vis spectra of Bi^{3+}-SnO_2 nanocomposite with Bi^{3+} mass ratios of 0% (grey), 4% (red), and 8% (green).

Figure 5 presents the variation of $(\alpha h\nu)^2$ with (hν) of all samples. The bandgap of the samples with Bi^{3+} concentrations of 0, 4, and 8% had values of 3.60, 3.16, and 2.55 eV, respectively. In the inset, the bandgap width is shown to decrease with Bi^{3+} dopant concentration. This is explained by the presence of the Bi dopant, which could result in the formation of more extrinsic defective energy levels in the bandgap of SnO_2, thus yielding new energy levels in the nanoparticles. Therefore, *sp-d*

exchange interactions between band electrons and localised *d* electrons of the Bi^{3+} ions with electronic states in the Sn^{4+} ions. The *s-d* exchange interaction lowers the conduction-band edge, but the virtual to *p-d* exchange interaction raises the valence-band edge, resulting in bandgap narrowing [6, 25]. The samples with 4 and 8% Bi^{3+} doping exhibited a red shift. This showed that the incorporation of Bi^{3+} dopant into the SnO_2 lattice made the absorption wavelength band of the material expand to the visible region.

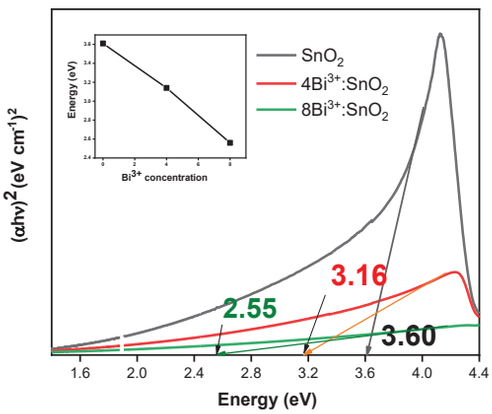

Fig. 5. Tauc's plots of pure SnO_2 and Bi^{3+}-doped SnO_2 with Bi^{3+} mass ratios of 0, 4, and 8%, respectively.

4. Conclusions

Bi^{3+}-doped SnO_2 nanocomposites with different Bi^{3+} concentrations were successfully synthesized by sol-gel and hydrothermal methods. Replacement of Sn^{4+} with Bi^{3+} in SnO_2 was confirmed by XRD, SEM, and UV-Vis diffuse reflectance spectroscopy. XRD analysis proved that all the samples were polycrystalline with diffraction lines assigned to the tetragonal rutile phases of SnO_2. The crystallinity of the samples decreased with the increase of Bi^{3+} dopant concentration. UV-vis spectra indicated that the bandgap of the materials decreased with increasing Bi^{3+} doping concentration thereby enlarging the light absorption range.

CRediT author statement

Thi Thu Hien Le: Data curation, Investigation, Conceptualization, Formal analysis, Writing- Reviewing and Editing; Van Tuan Chu: Conceptualization, Data curation; Van Tuan Pham: Supervision, Conceptualization, Formal analysis, Writing original draft.

COMPETING INTERESTS

The authors declare that there is no conflict of interest regarding the publication of this article.

REFERENCES

[1] Q. Schiermeier (2011), "Increased flood risk linked to global warming", *Nature*, **470**, DOI: 10.1038/470316a.

[2] S.N. Habisreutinger, et al. (2013), "Photocatalytic reduction of CO_2 on TiO_2 and other semiconductors", *Angew. Chem. Int. Ed.*, **52(29)**, pp.7372-7408.

[3] N. Manjula, G. Selvan (2017), "Magnetic and antibacterial properties of Zr-doped SnO_2 nanopowders", *Journal of Materials Science: Materials in Electronics*, **28**, pp.15056-15064.

[4] B. Wahlang (2018), "Exposure to persistent organic pollutants: Impact on women's health", *Rev. Environ. Health*, **33(4)**, pp.331-348.

[5] L. Ran, et al. (2015), "Highly crystalline Ti-doped SnO_2 hollow structured photocatalyst with enhanced photocatalytic activity for degradation of organic dyes", *CrystEngComm*, **17(22)**, pp.4225-4237.

[6] A. Baig, et al. (2020), "Facile synthesis of Ce-doped SnO_2 nanoparticles with enhanced performance for photocatalytic degradation of organic dye", *Journal of the Iranian Chemical Society*, **18**, pp.13-27.

[7] J. Wenk, et al. (2013), "Chemical oxidation of dissolved organic matter by chlorine dioxide, chlorine, and ozone: Effects on its optical and antioxidant properties", *Environ. Sci. Technol.*, **47(19)**, pp.11147-11156.

[8] L. Muruganandam, et al. (2017), "Treatment of waste water by coagulation and flocculation using biomaterials", *IOP Conference Series: Materials Science and Engineering*, **263**, DOI: 10.1088/1757-899X/263/3/032006.

[9] F. Liu, et al. (2020), "Microplastics removal from treated wastewater by a biofilter", *Water*, **12(4)**, DOI: 10.3390/w12041085.

[10] T.C. Jorgensen, L.R. Weatherley (2003), "Ammonia removal from wastewater by ion exchange in the presence of organic contaminants", *Water Research*, **37(8)**, pp.1723-1728.

[11] K. Singh, et al. (2017), "Heavy metal removal from wastewater using various adsorbents: A review", *Journal of Water Reuse and Desalination*, **7(4)**, pp.387-419.

[12] K.T. Alexei Pervov, N. Makisha (2018), "Application of reverse osmosis techniques to treat and reuse biologically treated wastewater", *IOP Conf. Series: Materials Science and Engineering*, **365(6)**, DOI: 10.1088/1757-899X/365/6/062026.

[13] D. Toloman, et al. (2020), "Enhanced photocatalytic activity of Co doped SnO_2 nanoparticles by controlling the oxygen vacancy states", *Optical Materials*, **110**, DOI: 10.1016/j.optmat.2020.110472.

[14] A. Alzamly, et al. (2019), "Tunable band gap of Bi^{3+}-doped anatase TiO_2 for enhanced photocatalytic removal of acetaminophen under UV-visible light irradiation", *Journal of Water Reuse and Desalination*, **9(1)**, pp.31-46.

[15] T. Karimi, et al. (2019), "Enhanced photocatalytic activity of SnO_2 NPs by chromium (Cr) concentration", *Bulletin of Materials Science*, **42(158)**, DOI: 10.1007/s12034-019-1842-0.

[16] S.S. Pan, et al. (2013), "Crystallite size-modulated exciton emission in SnO_2 nanocrystalline films grown by sputtering", *Journal of Applied Physics*, **113(14)**, DOI: 10.1063/1.4800896.

[17] J.A. Smith, et al. (2020), "Rapid scalable processing of tin oxide transport layers for perovskite solar cells", *ACS Appl. Energy Mater.*, **3(6)**, pp.5552-5562.

[18] G. Lucarelli, M.B. Thomas (2019), "Development of highly bendable transparent window electrodes based on MoOx, SnO_2, and Au dielectric/metal/dielectric stacks: Application to indium tin oxide (ITO)-free perovskite solar cells", *Frontiers in Materials*, **6(310)**, DOI: 10.3389/fmats.2019.00310.

[19] T.A. Dontsova, et al. (2020), "Enhanced photocatalytic activity of TiO_2/SnO_2 binary nanocomposites", *Journal of Nanomaterials*, **2020**, DOI: 10.1155/2020/8349480.

[20] I. Sayago, et al. (2019), "Development of tin oxide-based nanosensors for electronic nose environmental applications", *Biosensors (Basel)*, **9(1)**, DOI: 10.3390/bios9010021.

[21] N.S. Kumar, et al. (2019), "Silver quantum dot decorated 2D-SnO_2 nanoflakes for photocatalytic degradation of the water pollutant rhodamine B", *Nanomaterials (Basel)*, **9(11)**, DOI: 10.3390/nano9111536.

[22] L. Yang, et al. (2017), "Efficient hydrogen evolution over Sb doped SnO_2 photocatalyst sensitized by Eosin Y under visible light irradiation", *Nano Energy*, **36**, pp.331-340.

[23] P.S. Manjunathan, G.V. Shanbhag (2020), "Application of tin oxide-based materials in catalysis", *Tin Oxide Materials*, Elsevier, pp.519-553.

[24] T. Entradas, et al. (2014), "Synthesis of sub-5 nm Co-doped SnO_2 nanoparticles and their structural, microstructural, optical and photocatalytic properties", *Materials Chemistry and Physics*, **147**, pp.563-571.

[25] L.P. Chikhale, et al. (2014), "Effect of Bi doping on structural, morphological, optical and ethanol vapor response properties of SnO_2 nanoparticles", *Materials Science in Semiconductor Processing*, **27**, pp.121-129.

[26] S. Asaithambi, et al. (2019), "Preparation of SnO_2 nanoparticles with addition of Co ions for photocatalytic activity of brilliant green dye degradation", *Journal of Electronic Materials*, **48**, pp.2183-2194.

[27] B. Babu, et al. (2018), "One pot synthesis of Ag-SnO_2 quantum dots for highly enhanced sunlight-driven photocatalytic activity", *Journal of Alloys and Compounds*, **731**, pp.162-171.

[28] H. Chen, et al. (2013), "Synthesis and characterization of Ni doped SnO_2 microspheres with enhanced visible-light photocatalytic activity", *The Royal Society of Chemistry*, **5(69)**, DOI: 10.1039/C5RA10268E.

[29] M. Kandasamy, et al. (2018), "Ni-doped SnO_2 nanoparticles for sensing and photocatalysis", *ACS Applied Nano Materials*, **1(10)**, pp.5823-5836.

[30] C. Lu, et al. (2018), "Zn-doped SnO_2 hierarchical structures formed by a hydrothermal route with remarkably enhanced photocatalytic performance", *Ceramics International*, **44(13)**, pp.15145-15152.

[31] X. Meng, Z. Zhang (2015), "Facile synthesis of BiOBr/Bi_2WO_6 heterojunction semiconductors with high visible-light-driven photocatalytic activity", *Journal of Photochemistry and Photobiology A: Chemistry*, **310**, pp.33-44.

[32] X. Meng, Z. Zhang (2016), "Bismuth-based photocatalytic semiconductors: Introduction, challenges and possible approaches", *Journal of Molecular Catalysis A: Chemical*, **423**, pp.533-549.

[33] Z.F. Huang, et al. (2014), "Nanostructured bismuth vanadate-based materials for solar-energy-driven water oxidation: A review on recent progress", *Nanoscale*, **6(23)**, pp.14044-14063.

[34] L. Chu, et al. (2020), "Doping induced enhanced photocatalytic performance of SnO_2:Bi^{3+} quantum dots toward organic pollutants", *Colloids and Surfaces A: Physicochemical and Engineering Aspects*, **589**, DOI: 10.1016/j.colsurfa.2020.124416.

[35] A. Azam, et al. (2013), "Microwave-assisted synthesis of SnO_2 nanorods for oxygen gas sensing at room temperature", *Int. J. Nanomedicine*, **8**, pp.3875-3882.